

Communication

# Natural Flexible and Responsive 2D Photonic Materials with Micro-Sandwich Structure

Xijin Pan, Haoyang Chi and Gangsheng Zhang \* 

School of Resources, Environment and Materials, Guangxi University, 100 Daxue Road, Nanning 530004, China  
\* Correspondence: zhanggs@gxu.edu.cn

**Abstract:** Here, we report a two-dimensional (2D) amorphous photonic structure (APS) discovered in the central layer of the periostracum of the mussel *Perna canaliculus*, based on field emission scanning electron microscopy, X-ray diffractometer, attenuated total reflection Fourier transform infrared spectroscopy, and fiber optic spectrometry combined with the image processing technology and pair correlation function analysis. This APS contains ~29% in volume of protein fibers embedded in a protein matrix. These fibers, with diameters of  $103 \pm 17$  nm, are densely arranged and unevenly crimped. In addition, they are locally parallel with each other and exhibit short-range order with a nearest-neighbor distance of 189 nm. Interestingly, the APS is humidity-responsive with a vivid green structural color (~530 nm) in the wet state, which disappears in the dry state. Moreover, the APS is sandwiched by two dense layers in the periostracum, which is flexible in wet and can spontaneously or artificially deform into various shapes. We hope this APS may provide new inspirations for the design and synthesis of 2D amorphous photonic materials.

**Keywords:** periostracum; structural color; micro-sandwich structure; protein fibers; photonic device

## 1. Introduction

Natural photonic materials are defined as such materials that use nano-architectures (often called photonic structures) to produce striking optical effects in the human visible spectrum [1,2]. These photonic materials can be directly used as optical sensors and/or serve as templates to make novel photonic materials [3,4]. The latter shows important technical applications in solar energy manipulation and information technologies [5]. Therefore, we are interested in discovering and studying new photonic materials in living organisms.

Various natural photonic materials in organisms such as insects, birds, plants, and marine animals have been well reviewed in the literature [6–8]. Their nanostructures vary periodically or quasi-periodically in one- (1D), two- (2D), or three-dimensional (3D) directions and then are called 1D, 2D, or 3D photonic structures, respectively [9]. Comparatively, 2D photonic structures are less common in nature. To my knowledge, they only have been found in the spine of sea mouse [10,11], the feathers of peacocks and other bird species [12–14], the skin of birds and mammals [15,16], in comb rows of Ctenophores [17] and ligaments of bivalve animals [18–20]. Their structural colors are usually understood by scattering from fibrous structures coherently.

Molluscan shells can be simply divided into a two-layered structure: (1) The inner layer is CaCO<sub>3</sub> layer (such as the well-known mother of pearl), (2) the outermost layer covering the CaCO<sub>3</sub> layer is the most organic coating layer called the periostracum [21]. The latter is secreted by specialized cells called basal cells and stabilized by quinone tanning (an undefined process relating to protein cross-linking) [22]. Their formation, development, and functions have been well reviewed by Checa and Salas [22]. Moreover, the periostracum is multifunctional, such as waterproof, and acid-resistant, serving as a substrate for the deposition of the CaCO<sub>3</sub> layers [22,23]. Therefore, periostracum plays a key role in shell growth and survival.



**Citation:** Pan, X.; Chi, H.; Zhang, G. Natural Flexible and Responsive 2D Photonic Materials with Micro-Sandwich Structure. *Photonics* **2023**, *10*, 245. <https://doi.org/10.3390/photonics10030245>

Received: 28 November 2022

Revised: 14 January 2023

Accepted: 22 February 2023

Published: 23 February 2023



**Copyright:** © 2023 by the authors. Licensee MDPI, Basel, Switzerland. This article is an open access article distributed under the terms and conditions of the Creative Commons Attribution (CC BY) license (<https://creativecommons.org/licenses/by/4.0/>).

Mussels, such as blue mussel *Mytilus edulis* and green mussel *Perna canaliculus* are a type of ecologically and commercially important bivalve mollusk [24] with a particularly thick (5 to 428  $\mu\text{m}$ ) periostracum [25]. To date, for the *M. edulis* periostracum its structure has been extensively investigated and is well-known. Namely, the periostracum in *M. edulis* has an interesting sandwich structure with a middle vacuolated layer bounded by two dense layers [26]. In addition, this periostracum is composed of quinone-tanned sclerotized protein [26,27]. However, for the *P. canaliculus* periostracum its structure as well as composition has been little investigated and is largely unknown.

Here, we investigate the structure and composition of the *P. canaliculus* periostracum, particularly focusing on the origin of the green structure color found in the periostracum. We first find that this color results from an unusual fibrous photonic structure within the periostracum.

## 2. Materials and Methods

The green mussels *P. canaliculus* (length: 8–10 cm) were obtained from a commercial firm in Guangdong province, southern China. The samples were processed as follows: (1) The soft tissues were gently removed from the shell by a scalpel, (2) the shells were washed with distilled water and dried in air for 2 days, then dried in an oven at 35 °C for 12 h, (3) the shell was manually broken into fragments, (4) some fragments were decalcified with 3% HCl for 24 h to obtain the pure periostracum, which was then cut into strips and rinsed three times by distilled water, (4) the powder samples were prepared by scraping the shell and periostracum with a scalpel.

The optical images were taken with an optical (Optec MIT300) and Stereo microscope (Optec SZ66), both of which were equipped with a digital camera (Tucsen, Fuzhou, China, USB2.0, GT5.0). A halogen lamp (50 W) was used as the light source. In addition, the reflectance spectra were collected using an optical microscope (Optec MIT300) with a fiber optic spectrometer (AvaSpec-2048, Avantes, Broomfield, CO, USA) under normal incidence, during which a Teflon white reference tile (WS-2, Avantes) was used for reflectance calibration.

The power XRD patterns were collected with a diffractometer (Rigaku D/max-2500) using Cu Ka radiation ( $\lambda = 0.15406$  nm) at 40 kV (200 mA), which were analyzed using the software MDI Jade 6.0. Additionally, the attenuated total reflection Fourier transform infrared (ATR-FTIR) patterns were collected by an FTIR spectrometer (Bruker, Billerica, MA, USA, VERTEX 70) with a resolution of 4  $\text{cm}^{-1}$  and a range of 500 to 2000  $\text{cm}^{-1}$ .

SEM images were obtained with a field emission scanning electron microscopy (FE-SEM) (Hitachi, Tokyo, Japan, SU8020) operated at 10 kV and 10  $\mu\text{A}$ . Then, the images were processed using Quantitative Image Analysis (QIA-64) (Reindeer Graphics, Asheville, NC, USA), cooperated with Adobe Photoshop 2020 (Adobe, San Jose, CA, USA). Finally, the predicted reflectance spectrum was calculated by the Prum and Torres' Fourier tool as detailed elsewhere [28].

## 3. Results and Analysis

### 3.1. Optical Observation and Analysis

Figure 1A shows that the external surface is almost covered with a periostracum, which is absent near the umbo area. It generally shows nonuniform brown to dark colors. However, it shows a dim green color near the shell edge, which is called exterior green color in this work. It has the following basic characteristics: (1) It is limited only near the shell edge and on the external surface of the periostracum, (2) it is humidity-independent, i.e., both the dry and wet periostracum show identical green colors (Figure S1), (3) it is independent on both the incident and viewing angle (angle-independent) (Figure 1A). Therefore, this exterior green color is characteristic of chemical colors, which is beyond the scope of this work.

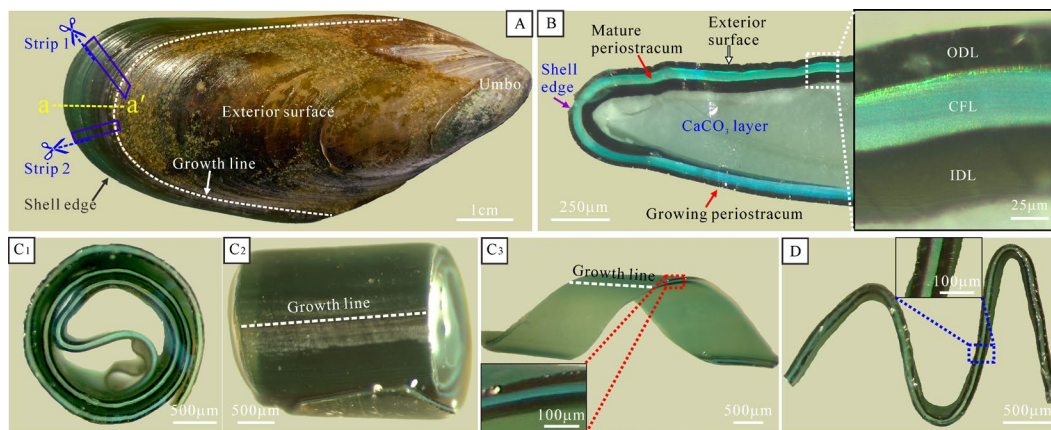


**Figure 1.** Optical images. (A) Exterior view of green mussel shell. (B) Cross-section of the shell at direction a-a' in (A). (C<sub>1</sub>, C<sub>2</sub>) Concentric spiral, (C<sub>1</sub>) cross-section view, (C<sub>2</sub>) top view, (C<sub>3</sub>) helicoid spiral. (D) Manually deformed letter. ODL: Outer dense layer, CFL: Central fibrous layer, IDL: Inner dense layer.

In cross-sections, the periostracum, which covers the CaCO<sub>3</sub> layers near the shell edge, can be divided into two parts: The growing periostracum located on the interior surface and the mature periostracum on the exterior surface (Figure 1B). The latter is the focus of this work and abbreviated as periostracum hereafter. Obviously, the periostracum has a tri-layer sandwich structure, of which the outer and inner layers show uniform dark brown color, while the central layer has bright nonuniform green colors (in set in Figure 1B). These three layers are called outer dense layer, inner dense layer, and central fibrous layer (CFL), respectively, based on the optical and SEM observations as will be detailed in the following Section 3.3.

It should be emphasized that the bright green color from the CFL has the following basic characteristics: (1) It occurs not on the surfaces of the periostracum but within it, namely, this green color cannot be observed unless the periostracum is broken, (2) it occurs in the entire periostracum, including the part of periostracum with brown surface color (Figure S2), (3) it is humidity-dependent, i.e., it only appears in the wet periostracum but disappears in the dry one (Figure S4). Therefore, the bright green color from the CFL is characteristic of the structural colors and clearly different from the exterior green color mentioned above. Please note this bright green color is the focus of this work.

Interestingly, as the periostracum is peeled away from the CaCO<sub>3</sub> layers and cut into rectangular strips oriented with different angles to the growth lines, these strips will spontaneously deform into various shapes, such as concentric (strip 2) and helicoid (strip 1) spirals with axes always parallel to the growth lines (Figure 1(C<sub>1</sub>–C<sub>3</sub>)). This should result from the relaxation of the residual stress in the periostracum. In addition, rectangular strips are highly flexible and can be manually deformed into arbitrary shapes, such as the letter M (Figure 1D).

### 3.2. XRD and FTIR Analysis

To evaluate the refractive index of PL, we carried out compositional analysis by XRD and ATR-FTIR. For the XRD patterns (Figure 2A), the full shell (including the periostracum and CaCO<sub>3</sub> layers) shows a series of sharp peaks superimposed with a broad peak at  $2\theta = 21^\circ$ . The former match well with those of aragonite (JCPDS no. 05-0453), and the latter indicates the existence of amorphous materials. In comparison, the periostracum shows only a broad peak at  $2\theta = 21^\circ$ . This provide further evidence that the periostracum is amorphous without any crystalline phases.

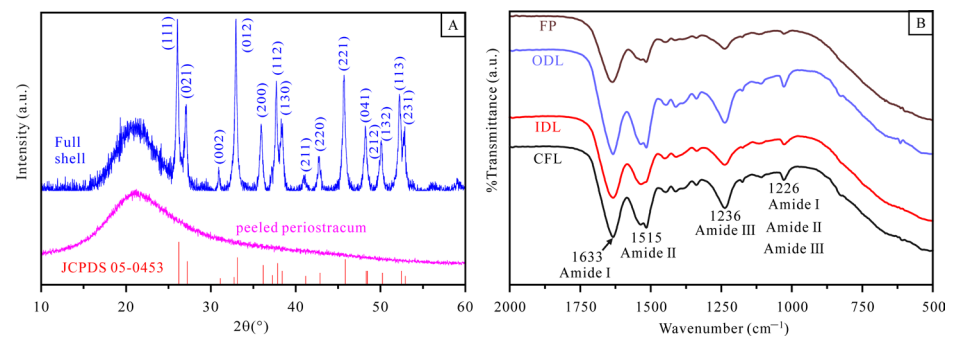
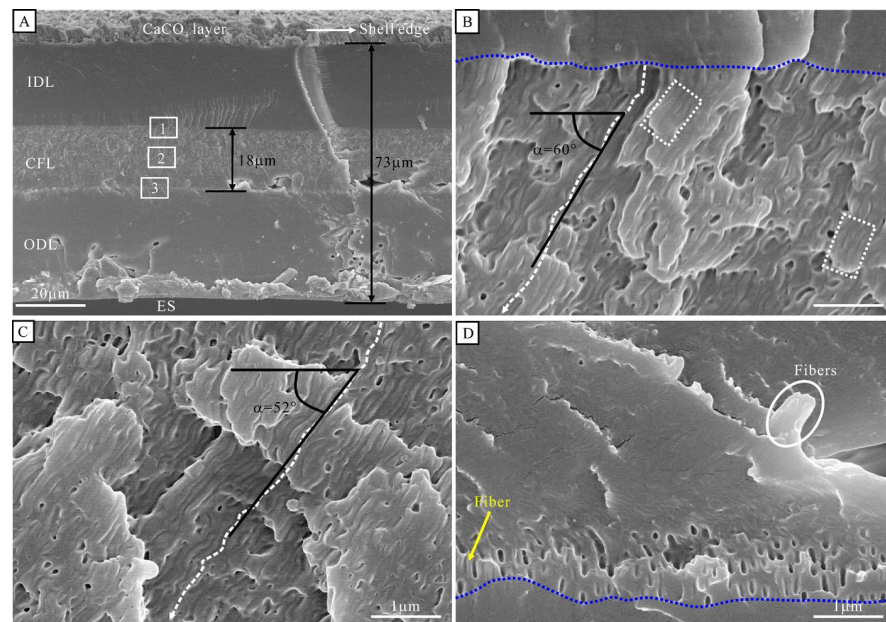


**Figure 2.** (A) XRD patterns of the periostracum and full shell. (B) The ATR-FTIR spectra of the periostracum. FP: Full periostracum, ODL: outer dense layer, IDL: Inner dense layer, CFL: Central fibrous layer.

For the ATR-FTIR spectra, the full periostracum and its corresponding three different layers show similar patterns. That is to say, all spectra show a prominent combination of peaks at  $1633\text{ cm}^{-1}$ ,  $1515\text{ cm}^{-1}$ ,  $1236\text{ cm}^{-1}$ , and  $1226\text{ cm}^{-1}$ , which are characteristic peaks of the proteins [29]. This means that the ODL, CFL, and IDL are of proteins, although their detailed composition and configuration should be different to some extent.

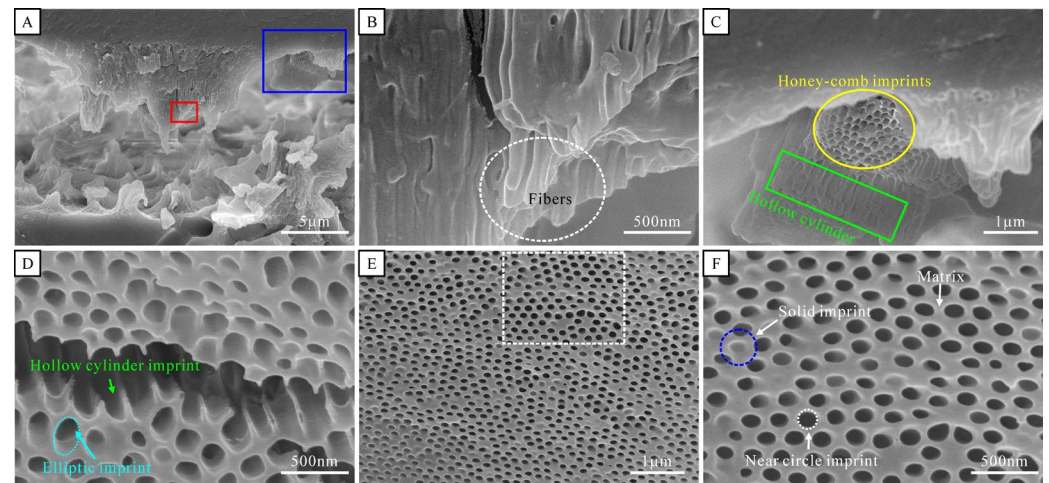
### 3.3. Structural Analysis

Figure 3 shows the SEM images of the periostracum in cross-section cut along the line a-a' in Figure 1A. At low magnification (Figure 3A), the periostracum consists of three layers: IDL, CFL, and ODL, similar to those under an optical microscope (Figure 1B). Among those, both the IDL and ODL appear homogeneous and dense thick layers with horizontal orientation. In contrast, the central layer (CFL) appears fibrous, consisting of bundles of crimped fibers (Figure 3C). Globally, their oblique angle  $\alpha$ , defined as the one between the fiber axis and shell exterior surface (ES), varies with regions. In more detail,  $\alpha$  is nearly vertical at the interfaces between the CFL and IDL (or ODL) (blue dashed lines in Figure 3B,D), while  $\sim 60^\circ$  in the top part of the CFL. However, locally,  $\alpha$  is nearly constant, meaning that adjacent fibers are parallel with each other (boxed areas in Figure 3B). Please note that the tri-layer structure occurs in the entire periostracum (Figure S3).



**Figure 3.** SEM images of an undamaged periostracum in cross-sectional fractured along the line a-a' in Figure 1A. (A) full view. (B–D) Detail of boxed areas 1, 2, and 3 in (A), respectively. ES: Exterior surface, ODL: Outer dense layer, CFL: Central fibrous layer, IDL: Inner dense layer.

Figure 4A–C shows the SEM images of the damaged periostracum in cross-section. At low magnification (Figure 4A), the fibers are severely curved, twisted, or broken. Interestingly, in some fractured surfaces, the fibers are still parallel with each other and projected outward (Figure 4B). However, in some fractured surfaces, the fibers are absent, and the numerous cavities are observed to be arranged like a honeycomb (Figure 4C). These cavities correspond to the imprints left by the fiber pull-out during fracturing (Figure 4D), which was evidenced by the fact that the diameter of the fibers and cavities are comparable, which are  $81 \pm 25$  ( $n = 58$ ) and  $103 \pm 17$  ( $n = 980$ ), respectively. In addition, during fracturing, some fibers are disrupted exactly at the fracture surfaces, leaving solid imprints (circles in Figure 4F).



**Figure 4.** (A–C) SEM images of the damaged periostracum in cross-section fractured along the line a–a' in Figure 1A. (A) Overview (B,C) the magnified image of the red box and the blue box in (A), respectively. (D, E) Sections fractured along the directions oblique or perpendicular to the fiber axes. (F) The magnified image of the white dashed box in (E).

On the other hand, the imprints in cross-sections look like near circular or elliptic shapes with slight irregularity, probably resulting from the deformation or nonuniformity of the global orientation of the fibers (Figure 4D–F). Essentially, its shapes depend on the relative orientation between the fibers and the fractured surface. That is to say, they may appear as hollow cylinders, circles, or elliptic when the fibers are parallel, perpendicular, or oblique to the fractured surface, respectively.

To analyze Figure 4E quantitatively, we used the software Quantitative Image Analysis (QIA-64) to transform it into a binary image (Figure 5A). Then, the fiber coordinates of centroids and sizes were extracted by QIA for  $g(r)$  and size analysis. The results of image analysis suggest that the fibers have a volume fraction of about 29% (Figure 5A), and their equivalent diameter is highly uniform with an average of  $103 \pm 17$  nm ( $n = 980$ ) (Figure 5B). The  $g(r)$  curve of fiber centroids shows a strong first peak at  $r = 189$  nm, which suggests the fibers are arranged in short-range order with a nearest-neighbor distance ( $d = 189$  nm) (Figure 5C). In conclusion, the image analysis proved that the CFL of *P. canaliculus* possesses a 2D amorphous photonic structure (APS) made up of proteinous fibers and matrix.

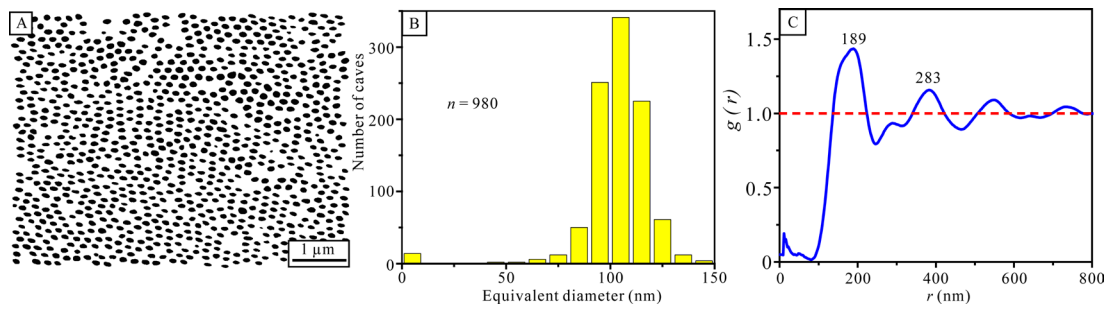


**Figure 5.** (A) Binary image of Figure 4E. (B) Histogram of the distribution of fibers’ equivalent diameter. (C) Pair correlation function of fiber centroids.

### 3.4. Spectral Analysis and Theoretical Predictions

To measure the reflected color quantitatively, we carried out a spectral reflectance measurement under normal incidence. Figure 6A shows the bright green color from the wet CFL has a reflection peak at 528 nm, which shifts to 500 nm after being air-dried for 30 min and disappears after being oven-dried for 24 h at 35 °C. In addition, Figure 6A also shows the periostracum has a dark brown reflection peak at 678 nm. These results coincide with optical observation and analysis in Section 3.1.

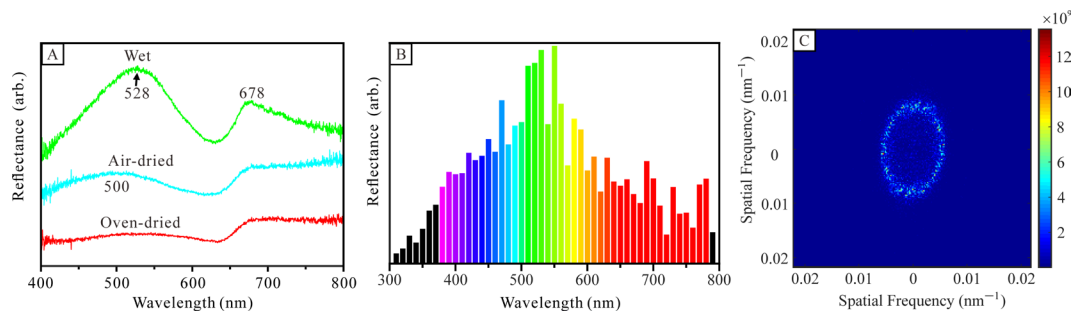


**Figure 6.** (A) Measured reflectance spectrum of cross-sectional fractured shell along line a-a’ in Figure 1A. (B) The predicted reflectance spectrum. (C) 2D Fourier power spectra of binary micrographs of nearly circular imprints.

To explore the peak position of structural green, we calculated the constructive reflection of CFL under normal incidence. When the wavelength of incident light matches the Bragg condition, a strong constructive reflection occurs and gives rise to a band gap centered at wavelength  $\lambda = 2n_{avg}d$ , where  $m$  is a positive integer,  $n_{avg}$  is the average refractive index, and  $d$  is the nearest-neighbor distance determined by the first strong peak of  $g(r)$ . For *P. canaliculus* CFL,  $d = 189$  nm and  $n_{avg}$  can be determined by Gladstone and Dale’s law [30]:

$$n_{avg} = n_p f_p + n_{m \cdot H} (1 - f_m)$$

where  $n_p$  is the refractive index of protein fibers ( $n_p = 1.56$  according to Ref. [31]), and  $f_p$  is the fiber volume fraction (29%).  $n_{m \cdot H}$  is the refractive index of the matrix containing water. To estimate  $n_{m \cdot H}$ , we assume that the refractive index of the dry matrix is very close to the protein fibers. We measured the lengths of CFL in dry and wet states, as shown in Figure S4, then  $n_{m \cdot H} = 1.56 \times \frac{29}{46} + 1.33 \times \left(\frac{46-29}{46}\right) = 1.48$ ,  $n_{avg} = 1.56 \times 29\% + 1.48 \times (1 - 29\%) = 1.5$ . Therefore,  $\lambda_{max} = 2n_{avg}d = 567$  nm.

Because the equation ( $\lambda = 2n_{avg}d$ ) cannot take amplitude variations into consideration, we try to show the shape of the reflectance spectrum using Prum and Torres’ 2D Fourier tool [28]. This tool can provide an accurate prediction for the shape of the reflectance spectrum of amorphous biological nanostructure. The refractive index of black and light materials is 1.48 and 1.56, respectively. The predicted result (Figure 6B) correctly reproduces the main features of the experiment and show a broad peak with a center at 535 nm, which is

in good agreement with the experimental observation, although there are some differences in shape. In addition, the Fourier power spectrum has a slightly ovoid pattern (Figure 6C), which suggests that the structure of CFL is nearly uniform in any direction (Figure 6C) [32]. In other words, the CFL possesses an isotropic band gap, which reflects non-iridescent green coloration coherently [32]. Based on the above results, we confirmed that the green color of CFL arises from 2D APS.

The theoretical prediction of the reflectance spectrum is carried out based on data from analyses of SEM images that require the sample are dry. However, the green is displayed in wet periostracum. Therefore, whether the length of periostracum changes after drying needs to be confirmed. Figure S4 indicates that inter-fiber space is constant when the periostracum attaches to the  $\text{CaCO}_3$  layer.

#### 4. Discussion

Many molluscan shells are well known for their beautiful color of mother of pearl (nacre), which is caused by the grooved surface or multi-layered microstructure (1D photonic structure) or both [33]. For the first time, we reported structural green in CFL of the periostracum of *P. canaliculus*, which arises from the 2D APS. In contrast to 2D photonic materials that have been found in animals [10–20], such as sea mice and peacocks, the photonic materials found in the periostracum of *P. canaliculus* are unique because (a) they have been packaged as a photonic device with ODL and IDL, (b) they are flexible (Figure 1D) and stretchable (Figure S4C,D). In contrast to those analogous engineered photonics materials [34,35], such as polymeric opal fibers, their compositional and structural complexity rarely captures the range of periostracum of *P. canaliculus*.

It is generally assumed that molluscan periostracum is among the strongest mechanically but most inert chemically in the animal kingdom [36]. The major reason is that it is a scleroprotein-containing structure, which forms through a chemical process called quinone tanning (i.e., forming protein cross-links) [26,27,36]. For periostracum *P. canaliculus*, the analysis results of its composition show that ODL, CFL, and IDL consist of identical protein materials. However, from the view of the degree of protein cross-links, it is obvious that both ODL and IDL are complete, but CFL is not, based on SEM observations. That is to say, the fibers of CFL are cross-linked, but the matrix is not. Moreover, we think the cross-linked degree of fiber of CFL is different between growing and mature periostracum. Therefore, we infer the diameter and space of fibers are different, which gives rise to the different colors of both, as shown in Figure 1B.

The universal phenomenon of natural photonic materials is their complexity and nonuniformity, especially in structure [2,6,37]. It is no exception for CFL of periostracum *P. canaliculus*. Its structural analysis shows that the diameter, separation, and direction of fibers continuously vary: (a) The diameter changes gradually along the axis of fiber, which is evidenced by that the diameter of the fibers in area 1, 2, and 3 (Figure 3A) are  $135 \pm 23$  nm ( $n = 11$ ),  $98 \pm 17$  nm ( $n = 12$ ), and  $75 \pm 9$  nm ( $n = 11$ ), respectively, (b) the separation between fibers inversely changes with diameter, which is evidenced by the fact that the space between fibers is constant (Figure S4), (c) globally, the oblique angle ( $\alpha$ ) varies from  $90^\circ$  to  $52^\circ$ , and then to  $90^\circ$ , locally, the adjacent fibers are parallel with each other, as described in Section 3.3. Thus, in this case, these continuous variations give rise to the nonuniform color appearance of CFL. For example, we think the enhanced green color near the ODL (Figure 1B) is mainly due to a greater refractive index difference [38] in area 3, where the content of the matrix is relatively high.

Please note that the predicted reflectance spectrum for natural photonic materials is generally limited in a local area due to their complexity and nonuniformity [28,39]. In this work, we choose a small area located in the middle CFL to make a prediction. Although it provides solid evidence that the 2D APS is responsible for the green color, our understanding of CFL's color-producing mechanism is still at an early stage. Therefore, more studies are needed, such as a more intensive theoretical study and using more advanced experimental ways (for example, FIB) of structure analysis in the future.

## 5. Conclusions

In cross-section, the central layer of periostracum of *P. canaliculus* has a bright green color. The cause of the color was studied via compositional and structural analysis of periostracum. The compositional analysis shows that the tri-layer periostracum is homogenous and protein. The structural analysis shows that the 2D amorphous structure comprised of fibers and matrix is responsible for the green color. Finally, we hope that this unusual 2D APS can provide new inspiration for the biomimetic structure of 2D photonic materials.

**Supplementary Materials:** The following supporting information can be downloaded at: <https://www.mdpi.com/article/10.3390/photonics10030245/s1>, Figures S1–S4.

**Author Contributions:** All authors contributed equally to this paper. All authors have read and agreed to the published version of the manuscript.

**Funding:** This research was funded by the National Natural Science Foundation of China (Grant No. 41762004).

**Data Availability Statement:** The data that support the findings of this study are available from the corresponding author upon reasonable request.

**Conflicts of Interest:** The authors declare no conflict of interest.

## References

1. Zhou, H.; Xu, J.; Liu, X.; Zhang, H.; Wang, D.; Chen, Z.; Zhang, D.; Fan, T. Bio-Inspired Photonic Materials: Prototypes and Structural Effect Designs for Applications in Solar Energy Manipulation. *Adv. Funct. Mater.* **2018**, *28*, 1705309. [CrossRef]
2. Mouchet, S.R.; Deparis, O. *Natural Photonics and Bioinspiration*; Artech House: Norwood, MA, USA, 2021; ISBN 9781630817978.
3. Ganter, P.; Lotsch, B.V. Photonic Nanoarchitectonics with Stimuli-Responsive 2D Materials. *Mol. Syst. Des. Eng.* **2019**, *4*, 566. [CrossRef]
4. Li, K.; Li, C.; Li, H.; Li, M.; Song, Y. Designable Structural Coloration by Colloidal Particle Assembly: From Nature to Artificial Manufacturing. *iScience* **2021**, *24*, 102121. [CrossRef] [PubMed]
5. Xuan, Z.; Li, J.; Liu, Q.; Yi, F.; Wang, S.; Lu, W. Artificial Structural Colors and Applications. *Innovation* **2021**, *2*, 100081. [CrossRef]
6. Kinoshita, S.; Yoshioka, S. Structural Colors in Nature: The Role of Regularity and Irregularity in the Structure. *Chem. Phys. Chem.* **2005**, *6*, 1442. [CrossRef]
7. Sun, J.; Bhushan, B.; Tong, J. Structural Coloration in Nature. *RSC Adv.* **2013**, *3*, 14862. [CrossRef]
8. Zhang, Z.; Chen, Z.; Shang, L.; Zhao, Y. Structural Color Materials from Natural Polymers. *Adv. Mater. Technol.* **2021**, *6*, 2100296. [CrossRef]
9. Greanya, V. *Bioinspired Photonics: Optical Structures and Systems Inspired by Nature*, 1st ed.; CRC Press: Boca Raton, FL, USA, 2015. [CrossRef]
10. Parker, A.R.; McPhedran, R.C.; McKenzie, D.R.; Botten, L.C.; Nicorovici, N.-A.P. Aphrodite's Iridescence. *Nature* **2001**, *409*, 36. [CrossRef]
11. Tayeb, G.; Gralak, B.; Enoch, S. Structural Colors in Nature and Butterfly-Wing Modeling. *Opt. Photon. N.* **2003**, *14*, 38. [CrossRef]
12. Zi, J.; Yu, X.; Li, Y.; Hu, X.; Xu, C.; Wang, X.; Liu, X.; Fu, R. Coloration Strategies in Peacock Feathers. *Proc. Natl. Acad. Sci. USA* **2003**, *100*, 12576. [CrossRef]
13. Pol Vigneron, J.; Colomer, J.-F.; Rassart, M.; Ingram, A.L.; Lousse, V. Structural Origin of the Colored Reflections from the Black-Billed Magpie Feathers. *Phys. Rev. E* **2006**, *73*, 021914. [CrossRef]
14. Lee, E.; Miyazaki, J.; Yoshioka, S.; Lee, H.; Sugita, S. The Weak Iridescent Feather Color in the Jungle Crow *Corvus Macrorhynchos*. *Ornithol. Sci.* **2012**, *11*, 59. [CrossRef]
15. Prum, R.O.; Torres, R. Structural Colouration of Avian Skin: Convergent Evolution of Coherently Scattering Dermal Collagen Arrays. *J. Exp. Biol.* **2003**, *206*, 2409. [CrossRef]
16. Prum, R.O.; Torres, R.H. Structural Colouration of Mammalian Skin: Convergent Evolution of Coherently Scattering Dermal Collagen Arrays. *J. Exp. Biol.* **2004**, *207*, 2157. [CrossRef]
17. Welch, V.; Vigneron, J.P.; Lousse, V.; Parker, A. Optical Properties of the Iridescent Organ of the Comb-Jellyfish *Beroë Cucumis* (Ctenophora). *Phys. Rev. E* **2006**, *73*, 41916. [CrossRef]
18. Zhang, G. Photonic Crystal Type Structure in Bivalve Ligament of *Pinctada Maxima*. *Chin. Sci. Bull.* **2007**, *52*, 1136. [CrossRef]
19. Zhang, G.S.; Huang, Z.Q. Two-Dimensional Amorphous Photonic Structure in the Ligament of Bivalve *Lutraria Maximum*. *Opt. Express* **2010**, *18*, 13361. [CrossRef]
20. Zhang, W.; Zhang, G. A Humidity Sensitive Two-Dimensional Tunable Amorphous Photonic Structure in the Outer Layer of Bivalve Ligament from Sunset Siliqua. *Mater. Sci. Eng. C* **2015**, *52*, 18. [CrossRef]
21. Sun, J.; Bhushan, B. Hierarchical Structure and Mechanical Properties of Nacre: A Review. *RSC Adv.* **2012**, *2*, 7617. [CrossRef]

22. Checa, A.; Salas, C. Treatise Online No. 93: Part N, Revised, Volume 1, Chapter 3: Periostracum and Shell Formation in the Bivalvia. *Treatise Online* **2017**, 84–100, 93:1–51. [[CrossRef](#)]
23. Meenakshi, V.R.; Donnay, G.; Blackwelder, P.L.; Wilbur, K.M. The Influence of Substrata on Calcification Patterns in Molluscan Shell. *Calcif. Tissue Res.* **1974**, *15*, 31. [[CrossRef](#)] [[PubMed](#)]
24. Gosling, E. *Marine Bivalve Molluscs*, 2nd ed.; Wiley: New York, NY, USA, 2015; ISBN 9781119045212.
25. Harper, E.M. The Molluscan Periostracum: An Important Constraint in Bivalve Evolution. *J. Paleontol.* **1997**, *40*, 71.
26. Wählich, F.C.; Peter, N.J.; Abad, O.T.; Oliveira, M.V.G.; Schneider, A.S.; Schmahl, W.; Griesshaber, E.; Bennewitz, R. Surviving the Surf: The Tribomechanical Properties of the Periostracum of *Mytilus* Sp. *Acta Biomater.* **2014**, *10*, 3978. [[CrossRef](#)] [[PubMed](#)]
27. Waite, J.H.; Andersen, S.O. 3, 4-Dihydroxyphenylalanine (DOPA) and Sclerotization of Periostracum in *Mytilus edulis*. *Biol. Bull.* **1980**, *158*, 164. [[CrossRef](#)]
28. Prum, R.O.; Torres, R.H. Fourier Blues: Structural Coloration of Biological Tissues. In *Excursions in Harmonic Analysis*; Birkhäuser: Boston, MA, USA, 2013; Volume 2, p. 401. [[CrossRef](#)]
29. Zengqiong, H.; Gangsheng, Z. A New Structural Model of Bivalve Ligament from *Solen Grandis*. *Micron* **2011**, *42*, 706. [[CrossRef](#)]
30. Meek, K.M.; Dennis, S.; Khan, S. Changes in the Refractive Index of the Stroma and Its Extrafibrillar Matrix When the Cornea Swells. *Biophys. J.* **2003**, *85*, 2205. [[CrossRef](#)]
31. Land, M.F. The Physics and Biology of Animal Reflectors. *Prog. Biophys. Mol. Biol.* **1972**, *24*, 75. [[CrossRef](#)]
32. Prum, R.O.; Torres, R.; Williamson, S.; Dyck, J. Two-Dimensional Fourier Analysis of the Spongy Medullary Keratin of Structurally Coloured Feather Barbs. *Proc. R. Soc. Lond. B* **1999**, *266*, 13. [[CrossRef](#)]
33. Tan, T.L.; Wong, D.; Lee, P. Iridescence of a Shell of Mollusk *Haliotis Glabra*. *Opt. Express* **2004**, *12*, 4847. [[CrossRef](#)]
34. Finlayson, C.E.; Goddard, C.; Papachristodoulou, E.; Snoswell, D.R.; Kontogeorgos, A.; Spahn, P.; Hellmann, G.; Hess, O.; Baumberg, J.J. Ordering in stretch-tunable polymeric opal fibers. *Opt. Express* **2011**, *19*, 3144. [[CrossRef](#)]
35. Kolle, M.; Lee, S. Progress and opportunities in soft photonics and biologically inspired optics. *Adv. Mater.* **2018**, *30*, 1702669. [[CrossRef](#)]
36. Waite, J.H. Quinone-tanned scleroproteins. In *Metabolic Biochemistry and Molecular Biomechanics*; Academic Press: Cambridge, MA, USA, 1983; p. 467. [[CrossRef](#)]
37. Ren, J.; Wang, Y.; Yao, Y.; Wang, Y.; Fei, X.; Qi, P.; Lin, S.; Kaplan, D.L.; Buehler, M.J.; Ling, S. Biological material interfaces as inspiration for mechanical and optical material designs. *Chem. Rev.* **2019**, *119*, 12279. [[CrossRef](#)]
38. Lertvachirapaiboon, C.; Jirapisitkul, T.; Pienpinijtham, P.; Wongravee, K.; Thammacharoen, C.; Ekgasit, S. Air-gap-enhanced pearlescent effect in periodic stratified bilayers of *Perna viridis* shell. *J. Mater. Sci.* **2014**, *49*, 6282. [[CrossRef](#)]
39. Holt, A.L.; Sweeney, A.M.; Johnsen, S.; Morse, D.E. A highly distributed Bragg stack with unique geometry provides effective camouflage for Loliginid squid eyes. *J. R. Soc. Interface* **2011**, *8*, 1386. [[CrossRef](#)]

**Disclaimer/Publisher's Note:** The statements, opinions and data contained in all publications are solely those of the individual author(s) and contributor(s) and not of MDPI and/or the editor(s). MDPI and/or the editor(s) disclaim responsibility for any injury to people or property resulting from any ideas, methods, instructions or products referred to in the content.